Metalurgi (2021) 3: 103 - 108

METALURGI
Majalah Ilmu dan Teknologi
p-ISSN 0126-3188 | e-ISSN 2443-3926
ejurnalmaterialmetalurgi.lipi.go.id

EFFECT OF Mo DURING THE OXIDATION OF Ni20Cr-xMo ALLOYS AT 570 °C

Resetiana Dwi Desiati[1], Hubby Izzuddin[1]*, Shigenari Hayashi[2]
[a]Research Center for Physics, National Research and Innovation Agency
Gedung 440-442, Kawasan Puspiptek Serpong, Banten, Indonesia 15343
[b] Division of Materials Science and Engineering, Faculty of Engineering, Hokkaido University
N13, W8, Kitaku, Sapporo, Hokkaido, Japan 060-8628
*E-mail: hubb001@brin.go.id

Masuk tanggal : 02-12-2021, revisi tanggal : 24-12-2021, diterima untuk diterbitkan tanggal 28-02-2022

Abstrak

Telah diinvestigasi efek penambahan Mo ketika oksidasi dari paduan Ni20Cr-xMo pada suhu 570 °C selama 100 jam. Hasil penelitian menunjukkan bahwa kualitas performa oksidasi dari paduan Ni20Cr meningkat dengan penambahan Mo. Selama oksidasi, paduan tanpa Mo membentuk lapisan tipis NiO pada bagian luar dan lapisan tebal Cr2O3 yang disertai penetrasi ke dalam dari lapisan Cr_2O_3 dan area tanpa Cr. Terdapat juga pembentukan campuran Ni-Cr oksida diantara lapisan NiO dan Cr_2O_3. Sementara itu, pada paduan yang mengandung Mo, lapisan oksida yang terbentuk memiliki sebuah struktur ganda (duplex) dengan lapisan NiO di bagian luar dan lapisan Cr(Mo)-Cr-Mo di bagian dalam. Terdapat juga oksida dengan struktur poros di lapisan bagian dalam. Penambahan Mo pada paduan Ni20Cr-xMo mengakibatkan perubahan perilaku oksidasi dengan mendorong pembentukan NiO dan berkurangnya difusi ke dalam menuju Cr_2O_3. Tetapi, akan lebih banyak terbentuk oksida labil yang mudah menguap dan oksida dengan struktur poros jika dilakukan penambahan lebih banyak Mo yang akhirnya menurunkan ketahanan oksidasi dari paduan Ni20Cr.

Kata Kunci: Efek penambahan Molybdenum, oksidasi temperatur tinggi, paduan Ni20Cr

Abstract

The effect of Mo during the oxidation of Ni20Cr-xMo alloys at 570 °C for 100 h was investigated. The results revealed that the oxidation performance of the Ni20Cr alloys was increased by Mo addition. During the oxidation, the Mo-free alloy formed a thin NiO scale on the outer scale and a thick continuous Cr_2O_3 scale accompanied with inward Cr_2O_3 penetrations and a Cr-depleted zone. There were also mixed Ni-Cr oxides in between the NiO and Cr_2O_3 scale. While, on the Mo-containing alloys, the formed oxide had a duplex structure with a thick NiO scale on the outer scale and Cr(Mo)-Cr-Mo oxides on the internal scale. A porous oxide structure was also formed in the inner scale. The Mo addition on the Ni20Cr-xMo has affected their oxidation behavior by promoting the formation of NiO scale and less the inward diffusion into Cr_2O_3 scale. But, more volatile oxides and porous oxide structures would form with higher Mo addition, resulting in lower oxidation resistance for the Ni20Cr alloys.

Keywords: *Effect of molybdenum, high temperature oxidation, Ni20Cr alloy*

1. INTRODUCTION

It is well known that the corrosion performance in an oxidizing atmosphere has strongly depended on the sustainability of formed protective of oxide layer continuously on the alloy surface, such as Cr_2O_3 or Al_2O_3, and some spinels [1]-[3]. Thus, at the waste-energy power plants that operate at high temperatures and chlorine-containing atmosphere, the coating materials were mainly selected from chromia/alumina forming alloys, such as NiCr, NiAl, NiCrAl, FeNiCr, FeCrAl-based alloys [2], [4]-[8].

Our previous study about the corrosion behavior of Ni20Cr-*x*Mo alloys in an oxidizing chlorine-containing atmosphere has exhibited that the corrosion performance was strongly influenced by the initial oxidation behavior of the Ni20Cr alloys [9].

DOI : 10.14203/metalurgi.v36i3.610
© 2021 Metalurgi. This is an open access article under the CC BY-NC-SA license (https://creativecommons.org/licenses/by-nc-sa/4.0/)
Metalurgi is Sinta 2 Journal (https://sinta.ristekbrin.go.id/journals/detail?id=3708) accredited by Ministry of Research & Technology, Republic Indonesia

It is very important to understand the oxidation mechanism and effect of alloying during the oxidation process to understand the corrosion mechanism in the oxidizing-chloridizing atmosphere. The alloying effect of Mo on the oxidation process at high temperature and dry air atmosphere has been studied on NiCr and FeCr-based alloys and showed the beneficial effect on increasing the oxidation resistance below 1000 °C [10]-[13]and the negative impact above 1000 °C [13]-[16]. This Mo formed volatile oxides during the oxidation process, such as MoO_3, which could degrade corrosion performance[16]-[17]. These volatile oxides depend on the concentration of Mo content and the oxidation temperature.

Therefore, the oxidation behavior of the Ni20Cr-*x*Mo alloys at 570°C will be more investigated in this study, including the effect of Mo addition.

2. MATERIALS AND METHODS

In this study, several samples of Ni20Cr-xMo alloys with different Mo contents (0, 1, 3, and 7 wt.%) were prepared with Ar arc-melting from metal powders with high purity. Then, to get fully γ phase, the alloy ingots were homogenized under vacuum at 1200 °C for 48 h. Samples were cut from the ingots with a thickness of approximately 1 mm. Then, the surface samples were prepared by mechanical polishing using SiC papers and 3 µm diamond paste. The samples were ultrasonically cleaned for 15 min before oxidation tests.

The cyclic oxidation tests were performed for up to 100 h at 570 °C in a muffle furnace under an air atmosphere. The oxidation mass gain was measured after 4, 9, 16, 25, 49, and 100 h at room temperature.

Due to a very thin formed oxide scale formed on the sample surfaces during the oxidation tests, the focused ion beam milling (JEOL JIB-4601F) was used to prepare cross-section samples. The oxide structure formed on the cross-section samples and mapping distribution of each element were examined and analyzed using FE-SEM-EDS JEOL, JSM-7001FA (field emission-scanning electron microscope- energy dispersive x-ray spectroscope). The depth profile distribution of each element formed on the oxide scales was analyzed using glow discharge optical emission spectroscopy (Jobin-Yvon 5000 RF) with radiofrequency (RF) of 13.56 MHz and power of 35 W. The oxide products' phase identification was analyzed using the XRD (x-ray diffraction) Rigaku SmartLab in the Bragg-Brentano geometry using Cu Kα1 radiation (λ = 0.15405 nm) in the range of 2090° with a step size of 0.02 and 4 s per step. To identify the structural phases from XRD patterns, the QualX2 software with the POW_COD database was used [18].

3. RESULTS AND DISCUSSIONS

3.1 Oxidation Kinetic

Figure 1 shows the oxidation kinetics of the Ni20Cr-*x*Mo alloys during the oxidation test. The mass oxidation gain of all Mo-containing alloys was lower than that of Mo-free alloy, indicating that Mo addition improved the oxidation performance of the Ni20Cr alloys. The lowest oxidation mass gain was obtained by the 1 Mo alloy, while with higher Mo addition up to 7 wt. % would increase the oxidation mass gain of the Ni20Cr alloys.

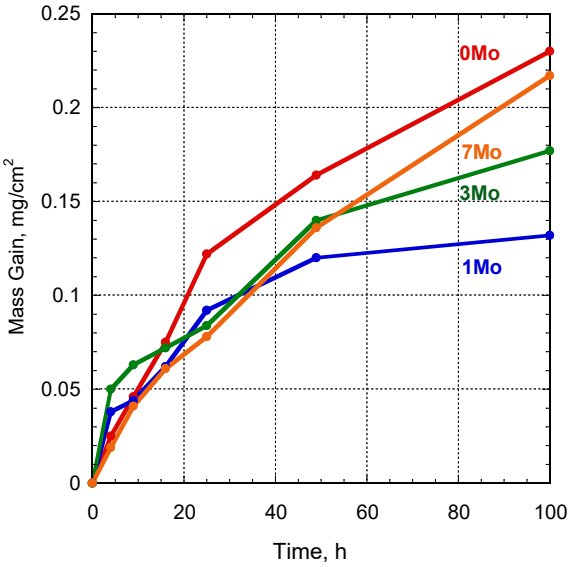

Figure 1. Oxidation mass gain of the Ni20Cr-*x*Mo alloys at 570°C for 100 h

All the kinetic profiles exhibited two stages of oxide growth: an early stage with a fast oxidation rate followed by a steady oxide growth. The Mo-free alloy profile displayed prolonged the early stage until 25 h, while the profiles of Mo-containing alloys showed quick the early stage between 4-9 h, with increasing the Mo content higher than 3 wt. %, the early stage with a fast oxidation rate was prolonged from 4 h to became 9 h.

3.2 Cross-Section Images dan EDS Mapping

The cross-section images of Mo-free alloy and 7 Mo-alloy after 100 h of oxidation at 570 °C were presented in Fig. 2 and Fig.3. These cross-sections were prepared by the FIB (focused ion beam milling) method. The cross-section images show that oxide scales formed on the Mo-free alloy were thicker than on the 7 Mo alloy, and

this is in accordance with the oxidation kinetic profile.

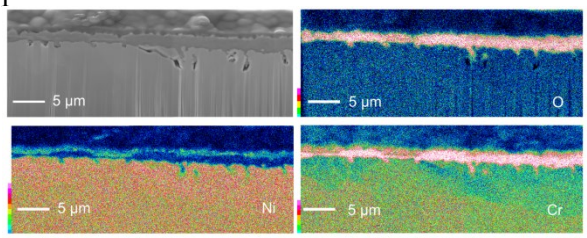

Figure 2. Cross-section of Mo-free alloy with elemental distribution maps after 100 hr of oxidation[9]

The oxide scales formed on the Mo-free alloy consisted of a single thick continuous Cr oxide (approximately 1.95 μm) accompanied with some inwards Cr oxide penetrations, as shown in Fig. 2. There was a very thin constant Ni oxide above the Cr oxide. It has also been observed that a Ni-Cr rich oxide was formed on most interface areas, while a Ni rich-Cr oxide was formed on small parts of the interface areas between Cr oxide and Ni Oxide. Similar structures were observed by L. Luo et. al., [19]. X.Yu et. al., [20] have also regarded this Ni rich-Cr oxide as metastable $Ni_{1-x}Cr_xO_{1-y}$ phase with 4 at% ~ 27 at% Cr doping. Beneath the Cr oxide penetrations, some voids and a Cr depleted zone were observed. The Cr depleted zone was formed due to the massive growth of the Cr oxide formation.

Meanwhile, the oxide scales formed on 7 wt.% containing alloy had a duplex oxide structure with a thick Ni oxide (around 1 μm) on the outer scale and an inner Cr rich oxide scale. The Mo oxide was observed in the inner layer and the Cr oxide. The inner layer was very porous in areas where the Mo was detected indicate that these oxides were volatile. The porous oxide structure was also observed in the previous study by D. Yun et. al., [10]. The formation of the volatile oxides is why the oxidation kinetic of 7 Mo alloy was higher than the 3 and 1 wt. % Mo-containing alloys, as discussed by N. Birks et. al., [17]

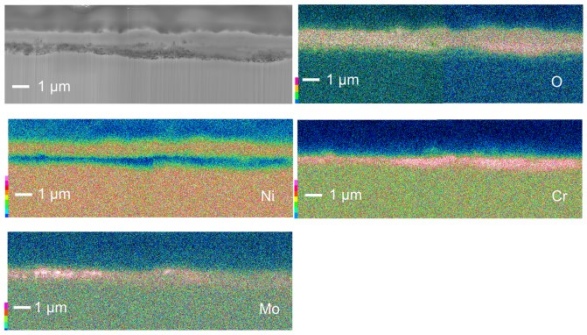

Figure 3. Cross-section of 7 Mo-alloy with elemental distribution maps after 100 hr of oxidation [9]

3.3 GDOS (Glow Discharge Optical Emission Spectroscopy) Depth Profile

To validate the FESEM-EDS observation, the oxide scales formed on Mo-free alloy and 7Mo alloy after 100 h of oxidation at 570 °C were examined using GDOES (glow discharge optical emission spectroscopy), which is shown in Fig. 4 as a depth profile distribution of each element.

The depth profile of Mo-free alloy shows that the structure of the oxide scale consisted of a Ni rich-Cr oxide on the outer scale oxide than followed by Cr oxide on the inner scale. Although the distance could not accurately measure the thickness of the oxide scale, the oxide structure information was similar to the FESEM-EDS (field emission-scanning electron microscope- energy dispersive x-ray spectroscope) result, as shown in Fig. 2.

Meanwhile, the depth profile of 7 Mo-alloy exhibited the duplex structure of a Ni oxide on the outer scale and a mix Cr-Mo oxide on the inner scale. Similar to the depth profile of Mo-free alloy, the depth profile of 7 Mo-alloy has the same structure which was observed on the FESEM-EDS image in Fig. 3.

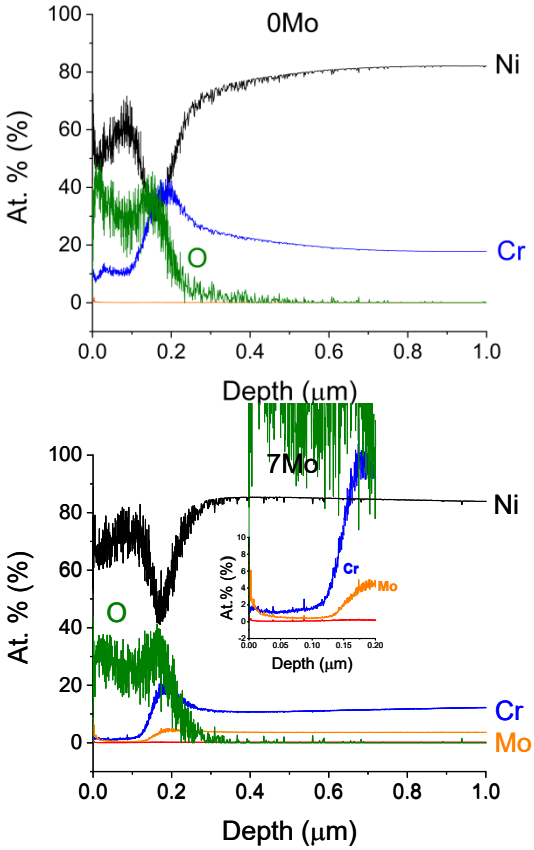

Figure 4. Depth profile of fomed oxide scales on the Mo-free and 7 Mo alloy samples after 100 hr of oxidation

3.4 XRD (X-Ray Diffration) Profile

Figure 5 shows the XRD (x-ray diffraction) profile of Ni20Cr-xMo alloys after 100 h of oxidation at 570 °C. The peaks of the XRD profile of Mo-free alloy were mainly detected as Cr_2O_3, NiO, Ni, and $NiCr_2O_4$. The Ni phase was initially from the substrate, thus the other phases were from the formed oxide scale. The Ni and Cr oxide formed on the oxide scale was confirmed as Cr_2O_3 and NiO from the XRD profile, respectively. The $NiCr_2O_4$ phase was correlated with the most areas of mixed NiCr oxide on the interface between NiO and Cr_2O_3, as shown in Fig. 3

Meanwhile, Cr_2O_3, NiO, Ni, and MoO_2 were detected on all peaks of the XRD profile of Mo-containing alloys. The NiO phase was correlated with the Ni oxide formed on the outer scale, while the Cr_2O_3 and MoO_2 were incorporated with a mix of Cr rich-Mo oxide formed on the inner scale.

The XRD results have confirmed the previously presented results from the FESEM-EDS images and the GDOES depth profiles.

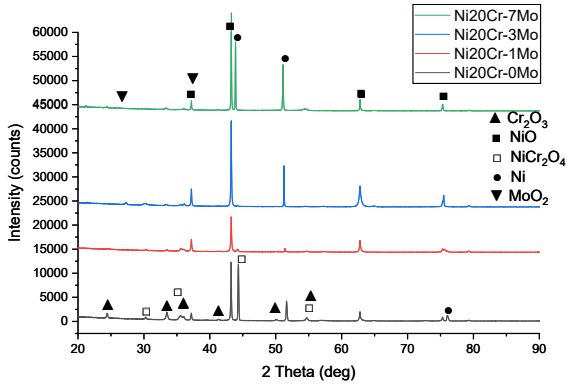

Figure 5. XRD profiles of the Ni20Cr-xMo alloys after 100 hr of oxidation

Unlike the Mo-free alloy, the outer scale formed on the 7 Mo-alloy consisted of Ni oxide only. This finding was elaborated from the XRD profile of Mo containing alloys that no NiCr oxide phase was detected, and only a very small amount of Cr on the outer scale (1-2 at. %) was detected from the inserted graph in the GDOES depth profile of the 7 Mo-alloy. Mo was also detected on the inserted graph, but with a more significant concentration than Cr instead (6 at. %). This result was found differently than from the previous studies [20]-[21]. The discovery of Mo on the outer scale might be why the Ni oxide formation on the outer scale of the 7 Mo-alloy was thicker than that formed on the Mo-free alloy. The Mo addition was able to promote the formation of Ni oxide during the oxidation process.

Figure 3 exhibited that the Mo EDS signal was influential, particularly on the right area of the inner scale but was less intense on other areas. On the regions with a strong indication of Mo, the porosity of the oxide scale was higher than that with a less severe Mo movement. Here, it might be that in these areas, a certain amount of Mo was doped on the chromium scale and reduced the oxygen vacancy, as explained by D. Yu et al. This Mo doping altered the chromium defect structure and suppressed the inward diffusion resulting in better oxidation performance [10].

$$2MoO_2 \xrightarrow{Cr_2O_3} 2Mo_{Cr}^{\circ} + 3O_O^X + \frac{1}{2}O_2 + 2e' \quad (1)$$

$$\frac{1}{2}O_2 + V_O^{\circ\circ} + 2e' \rightarrow O_O^X \quad (2)$$

$$Mo_{Cr}^{\circ} \rightarrow Mo_{Cr}^{\circ\circ\circ} + 2e' \quad (3)$$

This is why the oxidation resistance of Mo-containing alloys was better than that of the Mo-free alloy.

The effect of Mo doping by suppressing the inward diffusion will be less effective with higher Mo content, as shown on the XRD profile. The intensity of MoO_2 peaks was increased with higher Mo content in the Ni20Cr alloys (Fig. 5). More porous oxide structures on the inner scale might be more formed on the 3 and 7 Mo-alloys than 1 Mo-alloy due to a high volatile oxide of MoO_2. With these porous oxide formations, the chromium scale became less protective, leading to more Ni diffusion outwardly and a thicker NiO scale on the outer scale. This result has confirmed that the oxidation performance was decreased with increasing the Mo content on the Mo-containing alloys (see Fig. 1).

4. CONCLUSIONS

The oxidation study of the Ni20Cr-*x*Mo alloys at 570 °C has been analyzed thoroughly in this study. Based on the overall results, which have been explained above, it can be summarized that the mass oxidation gain of the binary Ni20Cr alloy was the highest. The oxide scale formed on

the binary Ni20Cr alloy consisted of a NiO scale on the outer scale and a thick Cr_2O_3 scale accompanied with inward Cr_2O_3 penetrations and a Cr-depleted zone. Mixed Ni-Cr oxides were formed in between NiO and Cr_2O_3 scale. Mo addition was effectively able to increase the oxidation resistance of the Ni20Cr alloys. The optimum Mo addition to the Ni20Cr alloys was 1 wt.%. The oxide scale formed on the Mo-containing alloys was a duplex structure with a thick NiO scale on the outer scale and Cr(Mo)-(Cr-Mo) combined oxides on the inner scale. A porous oxide structure was also formed in the inner scale. Mo addition has affected the oxidation behavior of the Ni20Cr-*x*Mo alloys by promoting the formation of NiO scale and suppressing the inward diffusion into the Cr_2O_3 scale. But, higher Mo addition would lead to more volatile oxides and porous oxide structures, resulting in lower oxidation resistance for the Ni20Cr alloys.

ACKNOWLEDGEMENT

The author was very grateful to the Nano - Micro Materials Analysis Division, and the High Voltage Electron Microscope laboratory-Graduate School of Engineering, Hokkaido University for all support during the characterization process used in this study.

REFERENCES

[1] M. Schütze, M. Malessa, V. Rohr, and T. Weber, "Development of coatings for protection in specific high temperature environments," *Surf. Coatings Technol.*, vol. 201, no. 7, pp. 3872-3879, 2006. Doi: 10.1016/J.SURFCOAT.2006.07.262.

[2] R. Bender and M. Schütze, "The role of alloying elements in commercial alloys for corrosion resistance in oxidizing-chloridizing atmospheres. Part II: Experimental investigations," *Mater. Corros.*, vol. 54, no. 9, pp. 652-686, 2003. Doi: 10.1002/maco.200303673.

[3] R. Jafari and E. Sadeghi, "High-temperature corrosion performance of HVAF-sprayed NiCr, NiAl, and NiCrAlY coatings with alkali sulfate/chloride exposed to ambient air," *Corros. Sci.*, vol. 160, p. 108066, 2019. Doi: 10.1016/j.corsci.2019.06.021.

[4] A. Zahs, M. Spiegel, and H. J. Grabke, "Chloridation and oxidation of iron, chromium, nickel and their alloys in chloridizing and oxidizing atmospheres at 400-700°C," *Corros. Sci.*, vol. 42, no. 6, pp. 1093-1122, 2000. Doi: 10.1016/S0010-938X(99)00142-0.

[5] R. Bender and M. Schütze, "The role of alloying elements in commercial alloys for corrosion resistance in oxidizing-chloridizing atmospheres. Part I: Literature evaluation and thermodynamic calculations on phase stabilities," *Mater. Corros.*, vol. 54, no. 8, pp. 567–586, 2003. Doi: 10.1002/maco.200390129.

[6] Y. Kawahara, Kawahara, and Yuuzou, "An overview on corrosion-resistant coating technologies in biomass/waste-to-energy plants in recent decades," *Coatings*, vol. 6, no. 3, p. 34, 2016. Doi: 10.3390/coatings6030034.

[7] E. Sadeghimeresht, L. Reddy, T. Hussain, N. Markocsan, and S. Joshi, "Chlorine-induced high temperature corrosion of HVAF-sprayed Ni-based alumina and chromia forming coatings," *Corros. Sci.*, vol. 132, pp. 170-184, 2018. Doi: 10.1016/J.CORSCI.2017.12.033.

[8] E. Sadeghi, N. Markocsan, and S. Joshi, "Advances in corrosion-resistant thermal spray coatings for renewable energy power plants. Part I: Effect of composition and microstructure," *J. Therm. Spray Technol.*, vol. 28, no. 8, pp. 1749–1788, 2019. Doi: 10.1007/s11666-019-00938-1.

[9] H. Izzuddin, S. Hayashi, S. Yoneda, T. Kogin, E. Ishikawa, and M. Noguchi, "Effect of Mo on corrosion behavior of Ni20Cr– x Mo alloys in air with NaCl–KCl–CaCl 2 vapor at 570°C," *Mater. Corros.*, vol. 71, no. 9, pp. 1488-1499, 2020. Doi: 10.1002/maco.201911469.

[10] D. W. Yun, H. S. Seo, J. H. Jun, J. M. Lee, and K. Y. Kim, "Molybdenum effect on oxidation resistance and electric conduction of ferritic stainless steel for SOFC interconnect," *Int. J. Hydrogen Energy*, vol. 37, no. 13, pp. 10328-10336, 2012. Doi: 10.1016/j.ijhydene.2012.04.013.

[11] A. Ul-Hamid, A. I. Mohammed, S. S. Al-Jaroudi, H. M. Tawancy, and N. M. Abbas, "Evolution of oxide scale on a Ni-Mo-Cr alloy at 900 °C," *Mater. Charact.*, vol. 58, no. 1, pp. 13-23, 2007. Doi: 10.1016/j.matchar.2006.03.005.

[12] H. J. Mathieu and D. Landolt, "An investigation of thin oxide films thermally grown in situ on Fe24Cr and Fe24Cr11Mo by auger electron spectroscopy and X-ray photoelectron

spectroscopy," *Corrosion Science*, vol. 26, no. 7. pp. 547-559, 1986. Doi: 10.1016/0010-938X(86)90022-3.
[13] N. Hussain, K. A. Shahid, I. H. Khan, and S. Rahman, "Oxidation of high-temperature alloys (superalloys) at elevated temperatures in air: I," *Oxid. Met.*, vol. 41, no. 3-4, pp. 251-269, 1994. Doi: 10.1007/BF01080783.
[14] F. A. Khalid, N. Hussain, and K. A. Shahid, "Microstructure and morphology of high temperature oxidation in superalloys," *Mater. Sci. Eng. A*, vol. 265, no. 1-2, pp. 87-94, 1999. Doi: 10.1016/S0921-5093(98)01181-2.
[15] J. L. González Carrasco, P. Adeva, and M. Aballe, "The role of microstructure on oxidation of Ni-Cr-Al base alloys at 1023 and 1123 K in air," *Oxid. Met.*, vol. 33, no. 1-2, pp. 1-17, 1990. Doi: 10.1007/BF00665666.
[16] L. Qin, Y. Pei, S. Li, X. Zhao, S. Gong, and H. Xu, "Role of volatilization of molybdenum oxides during the cyclic oxidation of high-Mo containing Ni-based single crystal superalloys," *Corros. Sci.*, vol. 129, no. May, pp. 192-204, 2017. Doi: 10.1016/j.corsci.2017.08.025.
[17] N. Birks, G. H. Meier, and F. S. Pettit, *Introduction to the high-temperature oxidation of metals*. Cambridge: Cambridge University Press, pp. 93, 2006.
[18] A. Altomare, N. Corriero, C. Cuocci, A. Falcicchio, A. Moliterni, and R. Rizzi, "QUALX2.0: A qualitative phase analysis software using the freely available database POW-COD," *J. Appl. Crystallogr.*, vol. 48, pp. 598-603, 2015. Doi: 10.1107/S1600576715002319.
[19] L. Luoa,L. Zou, D. K. Schreiber, D. R. Baer, S. M. Bruemmer, G. Zhou, C. M. Wanga, "In-situ transmission electron microscopy study of surface oxidation for Ni–10Cr and Ni–20Cr alloys," *Scr. Mater.*, vol. 114, pp. 129–132, 2016. Doi: 10.1016/j.scriptamat.2015.11.031.
[20] X. X. Yu, A. Gulec, C. M. Andolina, E. J. Zeitchick, K. Gusieva, J. C. Yang, J. R. Scully, J. H. Perepezko. L. D. Marks, "In situ observations of early stage oxidation of Ni-Cr and Ni-Cr-Mo alloys," *Corrosion*, vol. 74, no. 9, pp. 939–946, 2018. Doi: 10.5006/2807.
[21] A. Y. W. W. Lin, A. Müller, X. xiang Yu, A. M. Minor, and L. D. Marks, "Early-stage NiCrMo oxidation revealed by cryo-transmission electron microscopy," *Ultramicroscopy*, vol. 200, no. September 2018, pp. 6-11, 2019. Doi: 10.1016/j.ultramic.2019.01.012.